Combined Activated Carbon with Spent Fluid Catalytic Cracking Catalyst and MgO for the Catalytic Conversion of Waste Polyethylene Wax into Diesel-like Hydrocarbon Fuels

Piyaporn Kasetsupsin, Tharapong Vitidsant, Aminta Permpoonwiwat, Naphat Phowan, and Witchakorn Charusiri*

Read Online

ACCESS | 📊 Metrics & More | 📖 Article Recommendations | 🔵SI Supporting Information

ABSTRACT: Catalytic pyrolysis of polymer waste is an attractive alternative process for the conversion of large hydrocarbon compounds to useful products for the most reliable fueling and valuable chemicals, growing toward a circular economy and enhancing the reduction of waste materials. In this study, catalytic pyrolysis of waste polyethylene wax (WPEW) using a dual acid−acid catalyst and acid−base catalyst, which had various pore size distributions and included a strong active site, maximized the desirable yield and product distribution. The effect of the process conditions and synergy of activated carbon (AC) blended into both a spent fluid catalytic cracking catalyst (FCC) and magnesium oxide (MgO) catalyst was examined in a 3000 cm^3 custom-built reactor at varying operating temperatures (400−470 °C), inert

nitrogen gas flow rates (50 mL min^{-1}), catalyst loading (1−5 wt %), and FCC-AC and MgO-AC ratios in the catalytic conversion of WPEW to obtain the highest amount of diesel-like oil. The results indicated that thermal cracking of WPEW at 420 °C by a fixed inert N$_2$ flow rate of 50 mL min^{-1} obtained the highest liquid yield of 81.64 wt % and a diesel-like fraction of 35.51 wt %, while the catalytic conversion of WPEW under optimum conditions (temperature: 420 °C; fixed inert N$_2$ flow rate: 50 mL min^{-1}; catalyst load: 5 wt %; MgO-AC ratio: 0.5:0.5) achieved the highest liquid diesel-like yield of 41.92 wt %. Physicochemical analyses showed that the highest heating value of WPEW pyrolytic oil was 44.20 MJ kg^{-1}, and the viscosity was 1.7 mm^2 s^{-1} at 40 °C. The combination of MgO-AC as a dual catalyst illustrates a positive synergistic effect on the catalytic activity performance markedly, outstanding catalytic characteristics alongside high selectivity in pyrolysis of WPEW to paraffinic hydrocarbons in the diesel-like fraction.
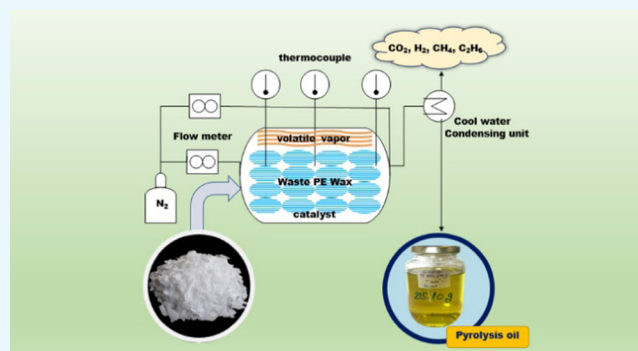
1. INTRODUCTION

Currently, the rapid global economic development and population growth pose worldwide challenges. Problems persisting in the environment due to an increase in waste, pollution, and an increase in greenhouse gas emissions affecting global warming and climate change have led to increasing interest in finding renewable energy that does not produce greenhouse gases, including the energy shortage crisis, and has been set as a target in several industries striving for sustainability. Developing alternative fuels through natural resources such as biomass or recycled resources is an option that is gaining attention and is responsible for encouraging the efficient application of resources by reusing spent materials or recycling waste. This is done by converting waste into energy to reduce the constraints of the depletion of fossil fuel reserves, which has a relatively great impact on reducing greenhouse gas emissions. This circular economy has gained attention over the past decade and will play a significant role in a low-carbon society, and the global economic development regarding these

processes can alleviate environmental problems and maintain the world's natural resources. The use of plastic materials has grown drastically due to their necessity in daily life and has greatly increased municipal solid waste. Therefore, the thermochemical conversion of plastic waste to liquid fuels has been of particular interest in terms of both the bio-circular-green economy and sustainable development.[1,2] In particular, the polymerization of ethylene in the catalytic-slurry reactor during recycling and the depolymerization process may produce intermediate products that act as impurities, resulting in the appearance of waste polyethylene wax (WPEW), which

has the main constituent of alkane hydrocarbons in the range of C_{16}–C_{30} and contains slightly branched hydrocarbons[3] that affect the melting temperature of polymer chains, which is generally lower than the polymerization temperature.[4] Pyrolysis of waste plastic has attracted much attention for minimizing waste and has emerged as a promising technology for both waste management and energy production by thermochemical conversion of waste plastic, which is an efficient process for decomposing long-chain hydrocarbon polymers into smaller hydrocarbons and rearranging them by secondary reactions and further catalytic reactions to light hydrocarbons that can be used as liquid fuels.[4,5] Waste polyethylene wax (WPEW) can be converted into energy by the thermal degradation process, which favors the formation of lower hydrocarbon molecules that contain mainly alkanes in a wide range of carbon numbers into fuel and valuable chemicals. Moreover, the use of several catalysts in thermochemical processes, such as catalytic cracking, has been recognized to enhance both yield and good selectivity to a more appropriate boiling point range of hydrocarbon fuels through the thermal degradation of WPEW even at relatively low operating temperatures.[6,7] For this purpose, this polymer was converted into liquid fuels that mainly consisted of iso-paraffins and aromatics under an inert atmosphere at the operating temperature of 400–550 °C.[8−10]

Several strong Lewis acid catalysts or Lewis base catalysts, such as typical zeolite, silica-alumina, and fluid catalytic cracking (FCC), including a basic catalyst as well as dolomite, MgO, and CaO, are also applied to the reaction to reduce the energy activation and process conditions, enhancing both yield and fuel composition,[11−14] which contained aliphatic, aromatic hydrocarbon and noncondensable gases through thermal degradation and intermediate ions due to a random scission mechanism from alkanes by the strong Lewis catalyst. The presence of catalysts enhanced the C−H and C−C bond cleavage of large hydrocarbon chains into medium or small hydrocarbon molecules before further isomerization, oligomerization, cyclization, and aromatization reactions. In general, both the acidic active site and porosity play a role in the diffusion and decomposition of carbon−carbon bonds over the acid sites and porous surface structure of the catalyst to obtain small hydrocarbon compounds.[15] However, high-temperature conditions may result in carbonaceous properties on the catalyst surface and hinder catalyst surface disintegration, affecting catalyst deactivation.[16]

Commercially available HZSM-5 is an effective catalyst in hydrocarbon cracking processes but is considered to be expensive and costly to regenerate; thus, an even more practical and economical process involves the use of FCC, which is classified as waste, but it is also an active and inexpensive catalyst. However, the occurrence of coke deposits over FCC during catalytic reactions affects the deactivation of acid active sites and reduces the mass transfer in pores, and channels of catalysts are hindered.[17,18] Dolomite (DM) is readily available as a kind of natural mineral that is used as an absorbent and a low-cost catalyst. As a catalyst, DM contains many Lewis basic sites that appear as CaO and MgO, improving the strong catalytic activity, and DM is used as an effective catalyst to convert both oxygenated and carboxylic groups in large hydrocarbons into linear saturated/unsaturated hydrocarbons and gases. However, there is a limitation of catalytic deactivation when used under high-temperature operating conditions.[19] MgO is a low-cost effective base

catalyst for the pyrolysis of large hydrocarbon compounds via the carbanion mechanism into light hydrocarbons and enhances the hydrogenation of alkenes to obtain saturated hydrocarbon compounds.[20−22] Furthermore, the use of an activated carbon (AC) catalyst, which illustrates the acidic active sites, high porosity, and surface area enhancement of catalytic pyrolysis of large hydrocarbon molecules via carbocationic cracking enhances to formulate moderate hydrocarbon compounds in the diesel-like boiling point range, can be obtained through large-pore-size activated carbon catalysts.[21,22]

This study aimed to determine the effects of temperature, and the blending ratio of both FCC-AC and MgO-AC in the pyrolysis of WPEW were evaluated for their effect on both maximized liquid yield and composition in the diesel-like boiling point range. The physicochemical and fuel properties of pyrolytic oil were characterized to determine its suitability as a fossil fuel replacement. In addition, the synergistic effect of combining strong acid-weakly acidic catalysts with weakly basic catalysts was determined to investigate its possibility and appropriateness as a dual catalyst and significantly enhanced the production of diesel-like oil via carbocationic cracking and carbanion mechanisms, drawn regarding the benefits of converting hydrocarbon waste for the alternative fueling and valuable chemicals toward a circular economy and reduction of waste materials.

2. EXPERIMENTAL SECTION

2.1. Materials and Characterization. In this study, WPEW supplied by CWC Intertrade Co., Ltd. was used as a feedstock in thermal degradation and catalytic pyrolysis to liquid fuels. Prior to the test, thermogravimetric analysis/differential thermogravimetry (TGA/DTG) was conducted to determine the thermal decomposition and weight loss of WPEW from 40 to 800 °C using a heating rate of 10 °C min^{-1} and inert nitrogen gas flow rate of 50 mL min^{-1} conducted in a TGA/DTG Pyris Diamond instrument (PerkinElmer, U.S.A.), after purging the system with N_2 (30 mL min^{-1}) at 150 K for 1 h. Moreover, spent FCC (Star Petroleum Co., Ltd., Thailand), MgO (PanReac AppliChem, Germany), and AC (Chulalongkorn University, Thailand) were used as catalysts. Morphological analysis was conducted to determine the surface area, pore volume, and pore size from the nitrogen adsorption−desorption isotherms conducted at 77 K using an ASAP 2020 instrument (Micromeritics, Germany) after degassing in vacuum at 573.15 K for 3 h. X-ray diffraction (XRD) characterization of the catalyst was performed in the 2θ range of 10−90° (at a scanning rate of 5° min^{-1}) operating at 40 kV and 40 mA with Cu Kα radiation (λ = 1540.6 Å) using a D8 Advance X-ray diffractometer (Bruker Corp., Germany) to determine the XRD pattern, which was obtained while an S8 tiger X-ray fluorescence spectrometer (Bruker Corp., Germany) was used to determine the mineralogical composition.

2.2. Experimental Procedures. Before each experiment, WPEW was placed in a hot air oven for 1−2 h to remove moisture and then crushed and sieved into an average size distribution from 11.2 to 12.5 mm. In this study, both thermal degradation and catalytic reactions of WPEW were carried out in a 3000 cm^3 custom-built stainless-steel tube reactor (30 cm internal diameter × 60 cm reactor length) coupled with a condensing unit using a cool-water condensing system to condense volatile vapor into a liquid fraction under atmospheric pressure. Figure 1 illustrates the schematic
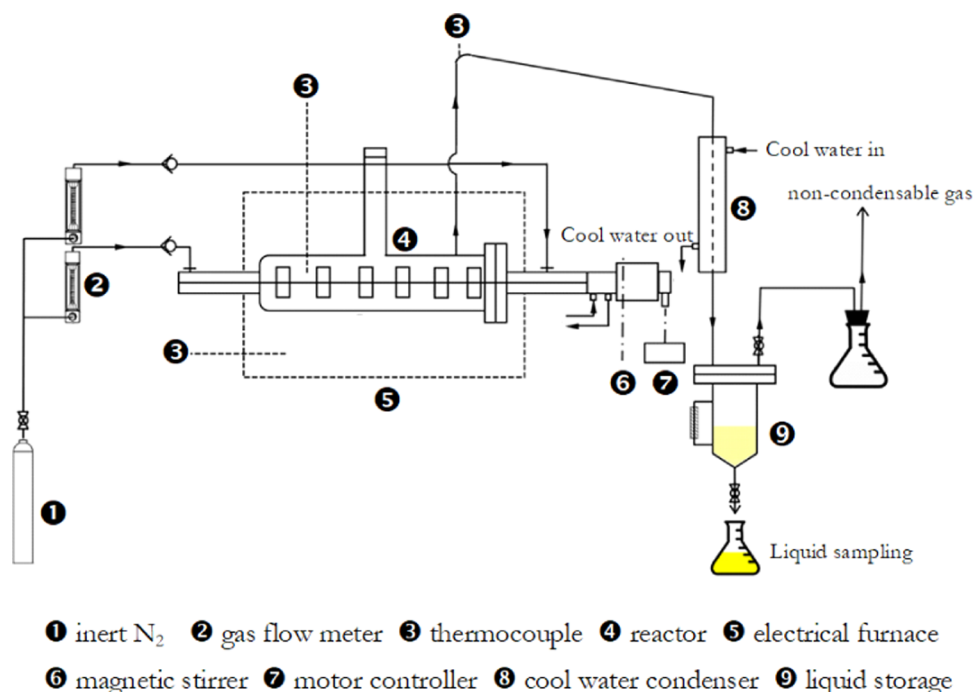
Figure 1. Schematic diagram of the bench-scale custom-built pyrolytic reactor.

diagram for the pyrolysis of WPEW into diesel-like liquid products. Prior to the test, the catalyst was added to the reactor at a load of 1−5 wt % of the feedstocks, and approximately 500 g of WPEW was added to the reactor. Inert nitrogen gas (50 mL min^{-1}) was fed into the reactor, ensuring that the experiment was conducted in an oxygen-free atmosphere. Then, a constant flow rate of 50 mL min^{-1} N$_2$ gas was used as the carrier gas in the pyrolysis reactions. A proportional-integral-derivative (PID) controller was preheated from ambient temperature to the predetermined temperature at 10 °C min^{-1}, and then the reactor was heated to the desired temperatures of 400, 420, 450, and 470 °C. Thereafter, the reactor was agitated by a magnetic stirrer at a fixed round per minute of 30 rpm to achieve a uniform heat/mass transfer, WPEW was decomposed into volatile vapor and passed through a cooling unit. Then, the pyrolyzed vapor was condensed from the entrained pyrolysis oil, which obtained the first drop to form pyrolysis oil until it was assured that the last drop of condensable volatile vapor had condensed, and the reaction was finished. The pyrolysis oil was collected in an oil collection tank, while the uncondensed gases were sampled and released into the atmosphere after collection. The solid residue was collected and weighed after the experiment and cooled at ambient temperature. The liquid pyrolysis oil and solid products were quantified by weighing, and the gaseous products were obtained by difference.

The yields of each product were defined as follows

$$Y_{liquid} = \frac{W_2}{W_1} \times 100 \tag{1}$$

$$Y_{solid} = \frac{W_4 - W_3}{W_3} \times 100 \tag{2}$$

$$Y_{gas} = 100 - (Y_{liquid} + Y_{solid}) \tag{3}$$

where W_1, W_2, W_3, and W_4 represent the weights of the feedstock, pyrolysis oil, catalyst, and total solid after pyrolysis, including long residuals obtained by depolymerization at high operating temperatures, respectively.

2.3. Product Characterization. The pyrolysis oil was analyzed using a Varian CP-3800 simulated distillation gas chromatograph (Varian, Inc., U.S.A.) coupled with an RTX2887 capillary column according to a simulated distillation of petroleum products (ASTM-D86) determined by the boiling points of the crude oil components as well as the distillate fraction from C$_5$ to materials that boil at approximately 200 °C are classified as naphtha-like, kerosene-like (200−250 °C), diesel-like (250−370 °C) and boiling point range over 370 °C, which are also classified as long residuals.[23] An Agilent GC-MS 7890/5978 instrument (Agilent Technologies, U.S.A.) and a nonpolar HP-5MS column coated with a 0.25 μm thickness film of 5% diphenyl and 95% dimethylpolysiloxane were used to identify the carbon number from the catalytic pyrolysis of waste PE wax. A volume of 1 μL of liquid oil was injected into the column with helium carrier gas at a flow rate of 1.5 mL min^{-1}, and the pyrolysis oil compounds were ionized at an ionization energy of 70 eV. The ion sources at 200 °C were identified with an m/z range of 40−700, and then the peak identification at several retention times was performed and compared with the mass spectral data library from the National Institute of Standard and Technology (NIST).

The physicochemical properties of pyrolyzed oil were determined according to the American Society for Testing and Materials (ASTM) standard, such as a higher heating value according to ASTM D240 using an AC-500 bomb calorimeter (LECO Corp., U.S.A.), the modified acid number (MAN) according to ASTM D664-07 using a 916 Ti-Touch automatic titrator (Metrohm AG, Germany) and the kinematic viscosity according to ASTM-D445 using a KV-6 viscometer bath (Stanhope-Seta, U.K.).

2.4. Synergistic Effect of Combining Acid−Acid Catalyst and Acid−Base Catalyst. To analyze the association of activated carbon blended with spent FCC and MgO during catalytic pyrolysis, the desirable product distribution on the pyrolysis products of WPEW was improved. The combination of experimental and theoretical values was determined as the difference between the experimental value and theoretical value.[24−26] The results illustrated the positive or negative effect of catalytic activity on the yield and product distribution, specifically pyrolysis oil in diesel-like form, through acid−acid catalysts and acid−base catalysts in eqs 4 and 5, respectively.

$$y_{\text{theoretical}} = y_{\text{AC}}\,AC_{\text{ratio}} + y_{\text{FCC}}\,FCC_{\text{ratio}} \tag{4}$$

$$y_{\text{theoretical}} = y_{\text{AC}}\,AC_{\text{ratio}} + y_{\text{MgO}}\,MgO_{\text{ratio}} \tag{5}$$

where AC_{ratio} is the activated carbon ratio, which was kept constant at 1.0, whereas FCC_{ratio} and MgO_{ratio} were varied from 0.25, 1.0, and 2.33 during catalytic experiments, and y_{AC}, y_{FCC}, and y_{MgO} are the yields from the experimental values obtained through catalytic pyrolysis of each catalyst alone.

$$y_{\text{difference}} = y_{\text{experimental}} - y_{\text{theoretical}} \tag{6}$$

In this paper, the $y_{\text{difference}}$ in eq 6 indicates the degree of synergy of the catalyst, which is divided into a positive synergistic effect $(y_{\text{difference}} > 0)$ and a negative synergistic effect $(y_{\text{difference}} < 0)$ occurring during catalytic pyrolysis using an acid−acid catalyst and acid−base catalyst.

3. RESULTS AND DISCUSSION

3.1. Characterization of WPEW. The TGA/DTG curves of the thermal degradation of WPEW are characterized by observing the weight change at a heating rate of 10 °C min^{-1} and under a N$_2$ atmosphere, as presented in Figure 2. The
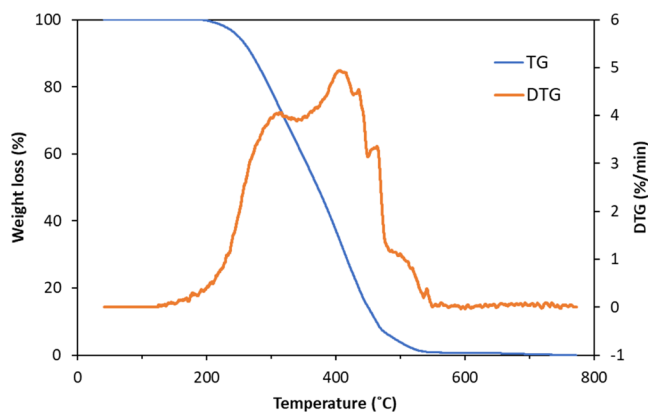

Figure 2. TGA/DTG of waste polyethylene wax.

decomposition of WPEW during thermal gravimetric analysis experiments can be mainly subdivided into two stages, which started at 220 °C and were nearly completed at 520 °C. The trends in weight loss curves obtained during TGA represented the physical and chemical structural changes occurring during thermal degradation. The DTG profile was divided into two distinct peaks. The first peak (formed at 310 °C) is reflected in a change in the mass of the sample. The first zone (280−300 °C) corresponds to the initial peak, which was probably due to thermal decomposition into a free radical and reveals radical intermediates where the middle long-chain hydrocarbon

compounds from different thermal degradation, such as thermal decomposition, depolymerization, and further cracking reactions, were the main stage of weight loss at the second peak (observed at approximately 420 °C). This had a higher decomposition intensity of 4.91 wt %/°C, corresponding to the degradation of the medium-length hydrocarbon chain into a small polymer chain, and further secondary cleavage within the 550−700 °C range of mass loss of WPEW was slightly changed due to the formation of solid char and ash. Therefore, the boundary of the catalytic pyrolysis experiment of WPEW was determined by varying the temperature range from 380 to 470 °C to obtain the highest liquid yield in carbon atoms ranging from C_{12}−C_{18}.

3.2. Characterization of the Catalysts. The XRD patterns (2θ range, 5−90°) of the spent FCC, MgO, AC, spent FCC-AC, and spent MgO-AC catalysts are shown in Figure 3. The XRD peaks of the spent FCC catalyst were weakened diffraction peaks at 2θ angles of 6.3, 10.3, 12.1, and 15.91°, in accordance with the diffraction of the (111), (220), (311), and (331) planes, respectively, were the characteristic peaks, which matched well with the standard zeolite Y phase (JCDPS No. 77-1551).[17] Additionally, a small amount of zeolite ZSM-5, Al$_2$O$_3$, and SiO$_2$ was observed. The spent FCC catalyst was mainly composed of stable zeolite Y that indeed has been used in cracking and hydrocracking catalysts and has an internal pore structure, an acidic site that promotes the C−C cleavage and hydrogen transfer affecting the degradation of large polymers to moderate compounds. Moreover, the porosity of spent FCC promotes the reaction of oligomerization, isomerization, and aromatization into the C_5−C_{12} range. The XRD patterns of MgO exhibit a high intensity at 2θ angles of 36.9, 42.9, 62.3, 74.8, and 78.6° in accordance with the diffraction of the (111), (200), (220), (311), and (222) planes, respectively, which exhibited the face-center-cubic MgO structure[27] (JCDPS No. 75-0447), while the intensity of the peaks was attributed to SiO$_2$ impurities. The AC exhibits very broad diffraction peaks, and the absence of a sharp peak reveals a predominantly amorphous structure. There are two broad diffraction peaks at approximately 2θ angles of 24 and 45°, in accordance with the diffraction of (002) and (100), respectively (JCPDS No. 41-1487).[28] The XRD results show that a combination of spent FCC-AC or spent MgO-AC catalysts exhibited the main diffraction peaks from each catalyst but showed that the diffraction peak was altered to a lower peak intensity when an additional catalyst was blended.

The main element compositions of spent FCC, MgO, and AC obtained by XRF are listed in Table 1.

Analyses of the N$_2$ adsorption−desorption isotherm of the catalyst are illustrated in Figure 4. The nitrogen gas adsorption−desorption was measured using the Brunauer−Emmett−Teller (BET) method. The textural properties of the spent FCC, MgO, AC, FCC-AC, and MgO-AC are illustrated in Table 2. The BET surface area ranged from 40.6 to 837.7 m^2 g^{-1}. It can be seen that the activated carbon exhibited the isotherm with the highest nitrogen gas adsorption volume across the P/P_0 range, thus having the highest BET surface area and pore volume with a BET surface area of 837.7 m^2 g^{-1} and a pore volume of 0.50 cm^3 g^{-1}. The blending of AC on the spent FCC (0.5:0.5 mass molar) exhibited a BET surface area of 620.5 m^2 g^{-1} and a pore volume of 0.41 cm^3 g^{-1}. BET analyses of spent FCC illustrated a BET surface area and pore volume of 111.9 m^2 g^{-1} and 0.16 cm^3 g^{-1}, respectively. In addition, the BET surface area and pore volume of MgO were

Figure 3. XRD pattern.
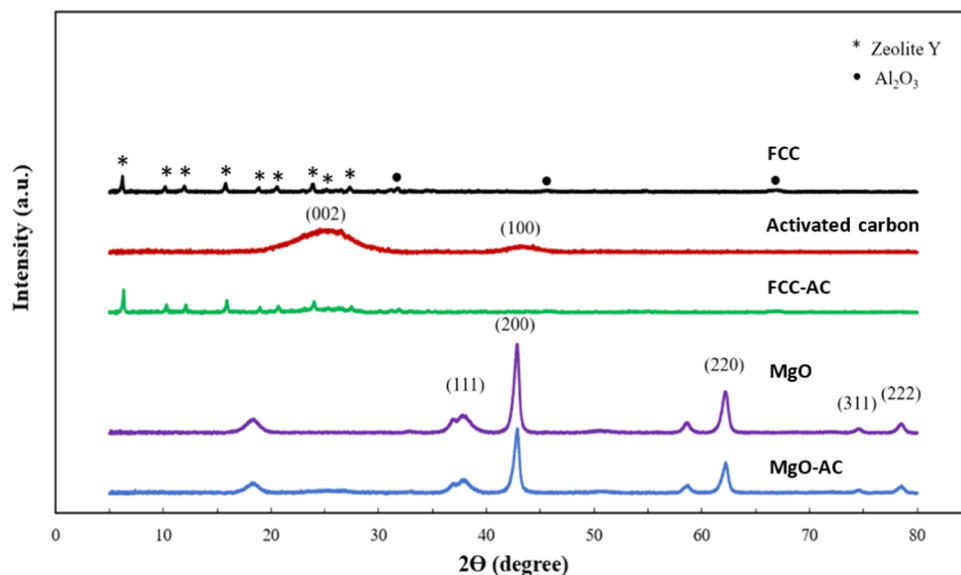
Table 1. XRF Analyses

	spent FCC				activated carbon				MgO		
element	wt %	oxide	wt %	element	wt %	oxide	wt %	element	wt %	oxide	wt %
Al	23.2	Al_2O_3	43.8	Al	1.12	Al_2O_3	1.82	Al	0.29	Al_2O_3	0.85
Si	18.5	SiO_2	39.6	Si	1.7	SiO_2	3.64	Si	0.24	SiO_2	0.72
Ti	0.44	TiO_2	0.72	Ti	0.09	TiO_2	0.2	Ti	0.02	TiO_2	0.06
Na	0.41	Na_2O	0.54	Na	0.38	Na_2O	0.64	Na	0.26	Na_2O	0.33
Ni	0.21	NiO	0.32	Ni	0.04	NiO	3.51				
Mg	0.19	MgO	0.3	Mg	0.4	MgO	0.67				
P	0.13	P_2O_5	0.27	P	0.09	P_2O_5	0.21	P	0.01	P_2O_5	0.02
Ca	0.08	CaO	0.12	Ca	0.46	CaO	0.02	Ca	0.23	CaO	0.29
S	0.05	SO_3	0.12	S	1.41	SO_3	0.15	S	0.02	SO_3	0.06
				Fe	1.27	Fe_2O_3	2.12				
				K	0.17	K_2O	0.51				
La	1.35	La_2O_3	1.58	La		La_2O_3					
Fe	0.5	Fe_2O_3	0.72	Fe		Fe_2O_3					
Ce	0.43	CeO_2	0.55	Ce		CeO_2					
V	0.11	V_2O_5	0.19	V		V_2O_5					
K	0.1	K_2O	0.13	K		K_2O					
				Mg		MgO		Mg	53.18	MgO	89.04
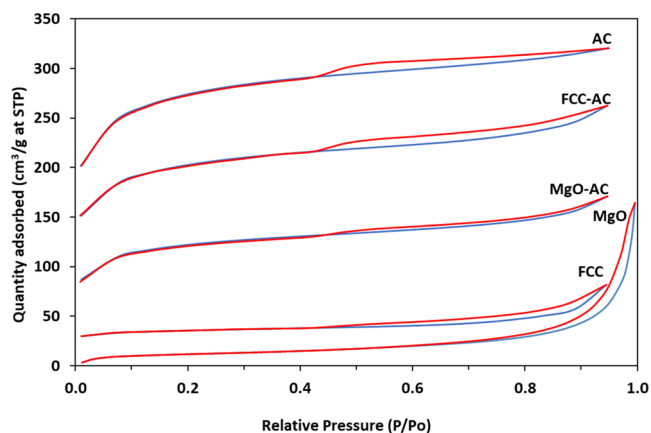
Figure 4. N_2 adsorption–desorption isotherms.

the lowest at 40.6 m^2 g^{-1} and 0.13 cm^3 g^{-1}, respectively. It is noteworthy that the blended catalyst tends to decrease the

Table 2. Textural Characteristics of the Catalyst

catalyst	total surface area (m^2 g^{-1})	total pore volume (cm^3 g^{-1})	average pore size (nm)
spent FCC	111.9	0.16	4.18
MgO	40.6	0.13	13.13
AC	837.7	0.50	2.37
FCC-AC	620.5	0.41	2.62
MgO-AC	377.4	0.26	2.86

BET surface and pore volume, and it was found that the pore size of the catalyst used in this study ranged from 2 to 50 nm, and the blended catalyst was classified as a mesoporous catalyst.

3.3. Product Yield and Product Distribution Analyses. *3.3.1. Effect of Operating Temperature.* The effects of the operating temperature and catalysts on the product distribution according to a noncondensable gas (C_1–C_4), a solid including repolymerized wax, and liquid (naphtha-like C_5–C_{12};
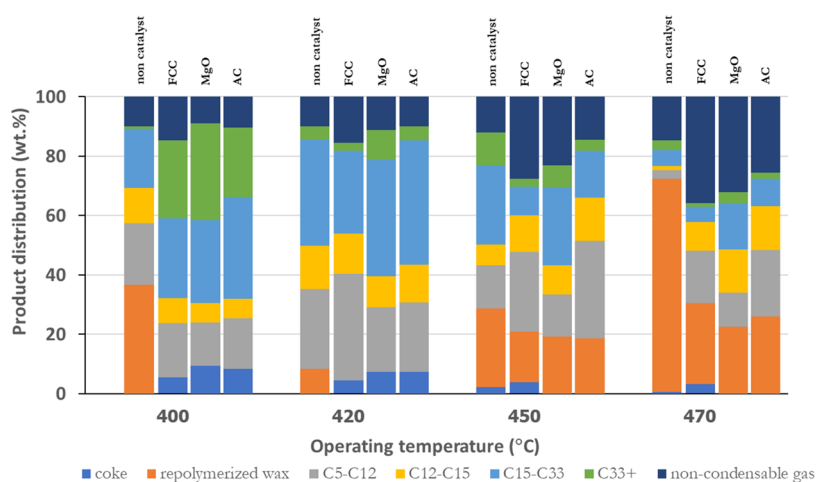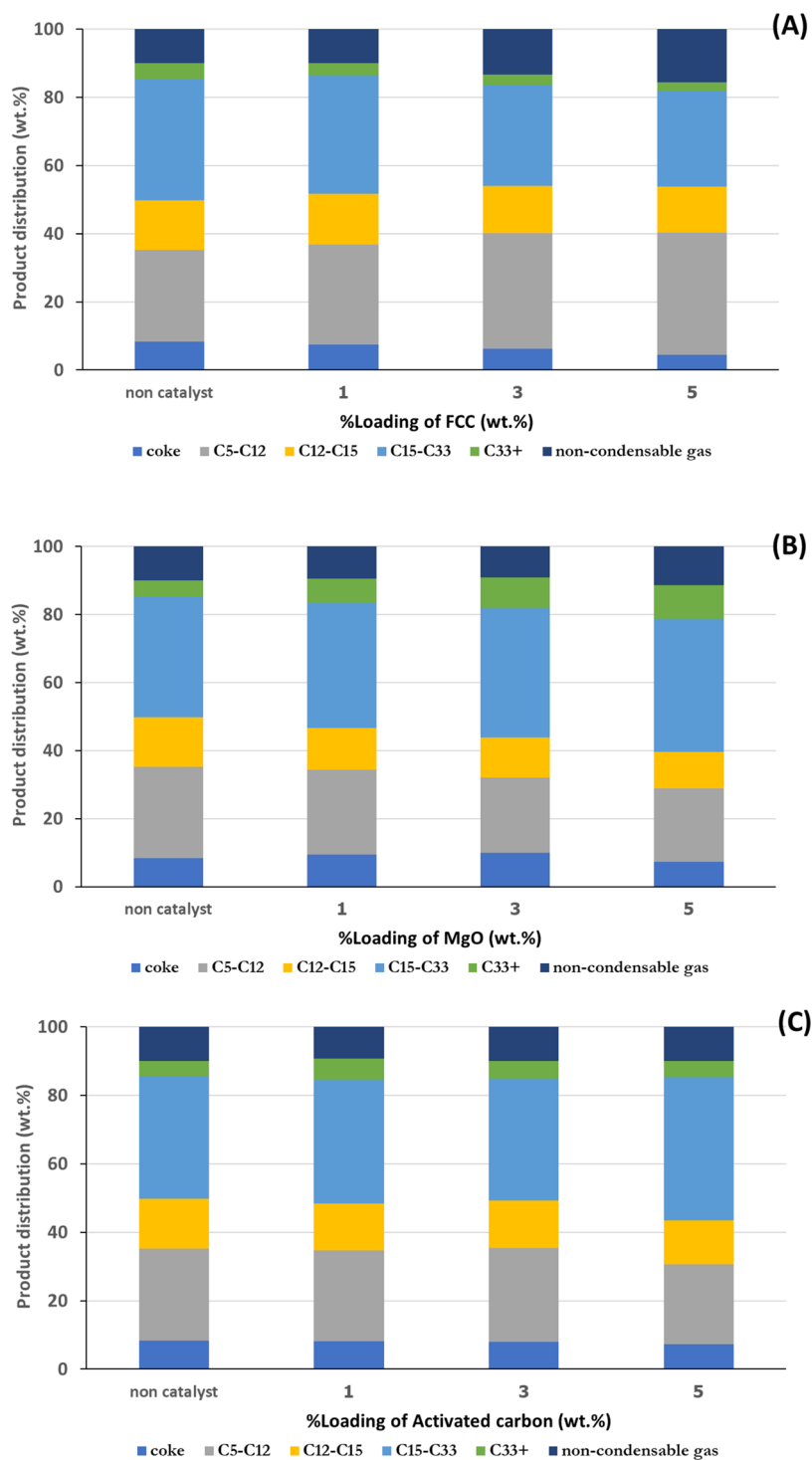
Figure 5. Effect of operating temperature from 400 to 470 °C at an inert N_2 flow rate of 50 mL min^{-1} with a 5 wt % loading of catalyst.

gas oil $C_{12}-C_{15}$; diesel-like $C_{15}-C_{33}$; long residue C_{33}^+) were investigated in this study. Figure 5 illustrates the effect of temperature from 400 to 470 °C on the product yield and product distribution of pyrolysis of WPEW with a noncatalyst and a comparison with several catalysts. In the noncatalytic pyrolysis test, the operating temperature mainly influences the thermal degradation of large hydrocarbon chains to medium and light hydrocarbon chains, which influence the radical degradation of the polymer chain. As the temperature increases, the van der Waals forces along the polymer chain are greater than the enthalpy of the carbon–carbon bonds enhanced to promote the decomposition of the polymer and volatilize the structure of the hydrocarbon chain. The results of the reaction temperature were increased from 400 to 470 °C, and the yield of the noncondensable gas increased from 9.98 to 14.71 wt %, in accordance with the primary thermal degradation that initiated a free radical affecting C–C bond cleavage to form the medium hydrocarbon chain, which was continuously influenced by the temperature until it underwent thermal decomposition in successive secondary cracking reactions. Further thermal degradation enhanced the decomposition of light hydrocarbon compounds to noncondensable gases, resulting in higher amounts of gaseous yield products. Moreover, it is worth noting that by increasing the operating temperature from 400 to 420 °C, the liquid yield increased from 53.44 to 81.64 wt % due to the heat transfer promoting the successive random breakdown of C–C bonds. Then, the β-scission cleavage of the hydrocarbon chain enhanced the degradation into shortened hydrocarbon chains and could further break down into smaller hydrocarbon molecules without polymerization reactions. Although the temperature was continuously increased from 420 to 470 °C, the liquid yield was dramatically decreased from 81.64 to 12.89 wt %, which can be explained by the high temperature promoting the cleavage of C–C bonds by initiating many free radicals to form small hydrocarbon compounds and obtaining a high proportion of noncondensable gas and repolymerizing wax of 26.56–71.89 wt % due to the secondary cracking reaction and accelerating the degradation of the hydrocarbon chains to smaller radicals, including the polymerization of long chains, which are still large-molecule volatile vapor compounds, to form a complex structure of polymer wax.[29,30] Analyses of product distribution according to the standard of distillation of petroleum products (ASTM D86) presented an increase in

operating temperature from 400 to 470 °C. The yield of the naphtha and kerosene range significantly decreased from 20.84 to 2.73 wt % and 11.92 to 1.43 wt %, respectively, whereas the yield in the diesel-like range increased from 19.83 to 35.51 wt % as the temperature increased from 400 to 420 °C and decreased to 5.31 wt % as the operating temperature increased to 470 °C. The results can be explained by the effect of temperatures of 400–420 °C enhancing the degradation of the polymer chain into radicals and the formation of smaller volatile vapor compounds with a longer retention time, which was caused by heat transfer in the reactor, affecting the successive thermal degradation of the polymer into shorter hydrocarbon compounds.[31] A higher naphtha yield was also obtained. At temperatures of 450–470 °C, the volatile vapor continuously decomposes into small radicals, and then the oligomerization and polymerization of medium-length hydrocarbon chains undergoing thermal breakdown are enhanced to form long-chain polymers. The operating condition of 420 °C obtained the maximum product distribution in diesel-like of 35.51 wt %, which was consistent with the thermal decomposition behavior by TGA/DTG analyses. Therefore, the operating conditions at the reaction temperature of 420 °C were suitable for use as the candidate pyrolysis temperature of WPEW to obtain liquid fuel products in the diesel range.

As seen in Figure 5, the effect of temperature from 400 to 420 °C on the product yield and product distribution from catalytic pyrolysis of WPEW obtained the product yield only in the solid, liquid, and gas fractions, whereas an increasing temperature tends to increase the repolymerized wax due to the volatile vapor undergoing degradation into a radical. Then, the oligomerization and polymerization of medium hydrocarbon chains are enhanced to form the long-chain polymer wax[29−32] as the process temperature increases from 450 to 470 °C. Furthermore, the yield of noncondensable gas increased as the temperature increased from 400 to 470 °C, especially the use of spent FCC as a catalyst, which also produced a greater proportion of noncondensable gas at 470 °C (35.82 wt %), consistent with the devolatilization being successive by increasing the reaction temperature. The highest liquid product yield (79.92 wt %) was attained at 420 °C and was reduced from 51.54 wt % (450 °C) to 33.66 wt % (470 °C) due to secondary thermal cracking, which continually degraded the liquid fraction to small-molecule hydrocarbon gases. Increasing the process temperature enhanced the catalytic

Figure 6. Effect of catalyst loading at an operating temperature of 420 °C and an inert N_2 gas flow rate of 50 mL min^{-1}: (A) spent FCC, (B) MgO, and (C) AC.

activity at the Brønsted acid site to degrade a medium-length chain into small hydrocarbon products, including the effect of pore selectivity at the pore surface structure,[16−18,32,33] which accelerated the formation of a small hydrocarbon gas. Catalytic pyrolysis using MgO and AC obtained gaseous yields of 32.19 and 25.62 wt %, respectively, under the same process conditions of 470 °C.

As depicted in Figure 5, the product distribution of the liquid product showed that the use of spent FCC obtained the highest naphtha fraction of 35.88 wt % at a temperature of 420

°C and tended to decrease (~17.69 wt %) by increasing the process temperature to 470 °C affected by the influence of high temperature accelerating the thermal decomposition to small free radicals, and the influence of stronger acid active sites enhanced the decomposition of small hydrocarbon compounds to produce a noncondensable gas. However, the temperature influence on the product distribution from pyrolysis of WPEW using MgO, in which the basic catalyst obtained a gas yield very close to pyrolysis using spent FCC due to the high temperature, is mainly affected by the thermal

degradation of the WPEW polymer into both small hydrocarbons and hydrogen radicals. Then, the influence of metal oxide MgO promotes hydrogen transfer[21,26,28,34] and carbon—carbon cleavage through mesoporous MgO into a moderate hydrocarbon chain, while the continual cracking reaction of the medium-length hydrocarbon compound produced a large amount of a noncondensable gas.[21,34] It was observed that the diesel-like content gradually increased from the increasing temperature of 420 °C, which maximized a diesel-like content of 39.01 wt % and decreased to 15.65 wt % at 470 °C, while a long residue (C_{32}^+) illustrated the same trend due to the influence of temperature and catalytic activity enhancing the conversion of WPEW into small hydrocarbon compounds. Both naphtha-like and kerosene-like compounds[21,26] also decreased to 11.47 and 14.45 wt % at 470 °C, which represented a large amount of noncondensable gas of 32.19 wt % causing thermal decomposition and further secondary cracking during the process.

The use of the AC catalyst in the pyrolysis of WPEW represented the effect of the temperature increase, which exhibited the same trend of product yield and product distribution. The obtained product yield consisted of solid (8.34−7.25 wt %), liquid (81.24−82.77 wt %), and a noncondensable gas (10.42−9.98 wt %) at a temperature increase from 400 to 420 °C, which was beneficial to convert the WPEW to the diesel-like fraction, thereby leading to an increase in the naphtha-like, kerosene-like and diesel-like fractions by the catalytic conversion of the large hydrocarbon structure. However, continuously increasing the temperature to 470 °C resulted in the undergoing of a secondary cracking of small hydrocarbons,[21,30,35] affecting the decrease in liquid yield and the enhancement of large polymers. The occurrence of repolymerized wax dramatically increased from 18.65 to 26.05 wt % as the temperature increased from 450 to 470 °C, in accordance with higher temperatures favoring the conversion of coke precursors to more condensed structures, which are still large structures, and these condensed structures formed a complex structure of large polymer wax at the water-cooling condensing unit. Considering both the product yield and distribution from catalytic pyrolysis of WPEW, it is optimal to operate at the process temperature of 420 °C.

3.3.2. Effect of Inert N_2 Flow Rate.
In this catalytic pyrolysis of WPEW, inert N_2 was used as a carrier gas to enhance the kinetics of the chemical reactants fed into the custom-built pyrolytic reactor. It is worth noting that the high flow rate of N_2 inert gas reveals the short residence time of volatile vapors and the insufficient heat transfer[29] from a heating source in successive cleavage of the C—C bonds of long-chain polymers into small hydrocarbon compounds in accordance with the previous literature,[36] due to a high flow rate of carried inert gas causing a shortening of the residence time in thermal cracking of large hydrocarbon compounds. Meanwhile, the active acid/base site of the catalyst could not rearrange the large hydrocarbon structure into a desirable hydrocarbon compound and pass them through the condensing unit coupled with a high flow rate of a carrier inert gas. Therefore, the N_2 flow rate was also correlated with the successive residence time in the pyrolytic reaction producing a desirable diesel-like fraction without the formation of repolymerized wax. This study was conducted using N_2 gas at 50 mL min^{-1} under the same conditions and correlation with the TGA/DTG analyses of WPEW.

3.3.3. Effect of Catalyst Loading.
The catalytic pyrolysis of WPEW under the process condition of 420 °C, inert N_2 of 50 mL min^{-1}, using the difference of catalyst loading from 1 to 5 wt % of feedstocks compared with the noncatalytic reaction is illustrated in Figure 6. The results showed that an increase in catalyst loading of the spent FCC from 1 to 5 wt % decreased the liquid yields and solid yield from 82.56 to 79.92 wt % and from 7.44 to 4.50 wt %, respectively. The significant change in gaseous yield also increased from 10.00 to 15.58 wt %. The results indicated that the role of the strong Brønsted acid catalyst was enhanced to improve the catalytic activity to cleave C—C bonds from the medium-length hydrocarbon chain to smaller compounds, after which the effect of high temperature accelerated the secondary cracking reaction, resulting in a decrease in liquid yields and an increase in gas yields.[17,18] Furthermore, it is worth noting that the slight appearance of a carbonaceous layer increased with the increase in spent FCC to pyrolytic pyrolysis of WPEW due to the oligomerization and aromatization of alkanes in the catalyst pore structure. Compared with the use of spent FCC and noncatalytic pyrolysis, it was found that using spent FCC catalyst decreased both the liquid and solid yields, while the yield of gaseous compounds was increased due to the role of the FCC catalyst in thermal breakdown by free radicals at moderate temperatures enhancing the C—C degradation of the polymer chains into short hydrocarbon chains. Then, the role of spent FCC was enhanced by the reaction carbocation at the acid site on the catalyst with the Lewis acid site, and the Brønsted acid site promoted the easier decomposition of medium-length hydrocarbons and continually cracked to small hydrocarbon compounds. Noncondensable gases affected the decrease in liquids and solid yield, while the yield of the gas product increased. Furthermore, an increase in the loading percentage of spent FCC in the catalytic pyrolysis of WPEW increased both Lewis acid and Brønsted acid active sites, which consisted of strong acidity and was favorable for coke formation by mass transfer of small molecules through the external surface and hindering contact between the large structure and the active sites inside the catalyst, thereby accelerating the decomposition of volatile vapor into small hydrocarbon compounds and obtaining a greater product distribution in the gas yield.[15,17,20,23,32] The product distribution of the liquid product consisted of naphtha from 29.31 to 35.88 wt % by the use of spent FCC loading increased from 1 to 5 wt %, whereas kerosene, diesel, and long-chain residue contents decreased to 15.03−13.51, 34.51−27.97, and 3.72−2.56 wt %, respectively. The effect of the acidic sites in the metal oxides could facilitate the dehydration reaction of organic molecules, which could also promote the cleavage of the macromolecules into small ones.[26,28,34] When using a spent FCC loading of 1−5 wt %, it was found that using a spent FCC increased the product distribution in the naphtha-like range, while kerosene, diesel, and a long residue range also decreased due to the influence of the active site on the spent FCC enhanced to promote the dehydrogenation reactions, affecting an increase in the hydrogen transfer. Alkanes and alkenes produced by WPEW could undergo secondary cracking coupled with a role of strong acidity active sites in the cleavage of C—C bonds of a moderate hydrocarbon chain in the C_{12}−C_{32} range to the C_5−C_{12} range, and the product distribution in the diesel-like range was 35.88 wt %, which was similar to the product yields of thermal cracking under the same process conditions.
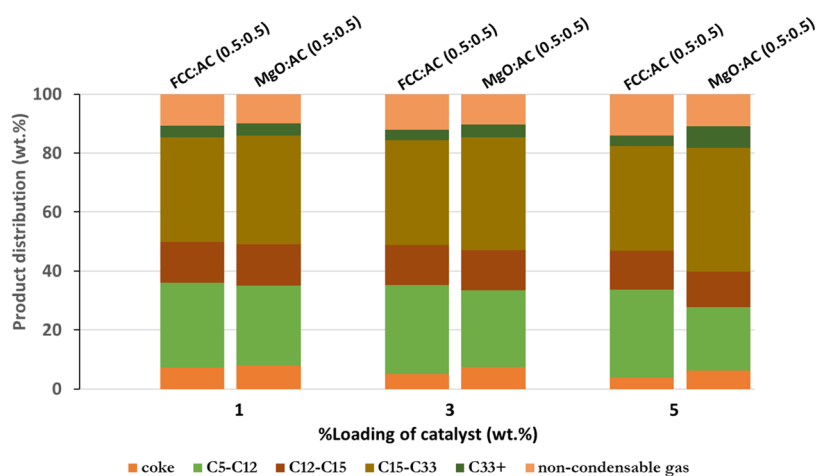
Figure 7. Comparison of the blended acid−acid catalyst and acid−base catalyst at various catalyst loadings at an operating temperature of 420 °C and an inert N_2 gas flow rate of 50 mL min^{-1}.

The use of MgO, a basic catalyst with a relatively large pore size, facilitated the formation of a medium-length hydrocarbon chain and affected the rapid contact time of pyrolytic volatiles on the catalyst surface, inhibiting the subsequent cleavage reaction of long-chain hydrocarbons and the alkaline center in the basic oxides could effectively promote the fracture of the C−H bonds and C−C bonds, accelerating the formation of gaseous products and correspondingly producing a large proportion of gas.[21,34] The effect of MgO loading on the catalytic pyrolysis of WPEW was tested from 1 to 5 wt %; the liquid yield obtained from the catalytic pyrolysis of WPEW slightly fluctuated from 81.05 and 78.96 to 81.32 wt % with increasing MgO loading from 1 to 5 wt % because the operating temperature facilitated the thermal degradation of WPEW to produce hydrogen radicals and short-chain hydrocarbon radicals and underwent hydrogenation with hydrogen radicals on the MgO surface,[20−22,34] which was succeeded by increasing MgO loading. It seems that an increase of MgO loading to 5 wt % achieved the highest conversion of WPEW to a liquid yield of 81.32 wt %, which consisted of naphtha-like, kerosene-like, diesel-like, and long residues contents of 21.59, 10.64, 39.01, and 10.07 wt %, respectively. Moreover, the solid yield slightly decreased from 9.43 to 7.35 wt %.

The effect of AC loading in catalytic pyrolysis of WPEW from 1 to 5 wt % indicated that an increase in the % loading of AC enhanced the slightly increased liquid and gas product yields, whereas the solid product yields tended to decrease with the use of 3 wt % AC loading. Furthermore, a comparison of thermal degradation and catalytic pyrolysis reactions showed that the use of an AC catalyst resulted in a greater liquid yield but also a decreased solid yield, which can be explained by the fact that the cleavage of C−C carbon occurred when the catalyst loading of AC was increased to increase the number of active sites; additionally, analyses of liquid product distribution showed that the effect of increasing the loading of AC from 1 to 5 wt % caused the naphtha-like, kerosene-like and long residue contents to decrease from 26.55 to 23.42 wt %, 13.73 to 12.83 wt % and 6.04 to 4.80 wt %, respectively. In contrast, the product distribution of diesel-like products also significantly increased from 36.18 to 41.72 wt %. The catalytic pyrolysis of WPEW using 5% AC loading obtained the highest diesel-like fraction of 41.72 wt %. The increasing catalyst

loading enhanced the thermal decomposition of WPEW and cleavage of C−C bonds to a medium-length hydrocarbon compound due to the activated carbon representing a weak Brønsted acid rather than a spent FCC, which engaged the mechanism of catalytic pyrolysis through the random scission of C−C to form a radical and a medium-length hydrocarbon. Then, the pore size with a high surface area of the activated carbon enhanced the degradation of the medium-length hydrocarbon compound undergoing cleavage at the active site and passing through the pore structure to rearrange and isomerization to produce a diesel-like compound, including facilitating the conversion of medium-length hydrocarbons into a noncondensable gas with a hydrogen radical reaction.[21,22,34,35]

3.3.4. Effect of AC Blending. The comparison of the blended acid−acid catalyst and acid−base catalyst with various total weights of catalyst loading at an operating temperature of 420 °C and an inert nitrogen gas of 50 mL min^{-1} is illustrated in Figure 7. In particular, the metal oxides affected the yields of the carbon range fraction including gaseous yield, the acidic oxides (from Al_2O_3, SiO_2, and ZnO in spent FCC and activated carbon), the yields of liquid over the catalysts containing those metal oxides were relatively higher due to the effect of metal oxides enhancing both of C−C bond and C−H bond cleavage into short hydrocarbon chains and continuing degradation to small compounds to obtain higher relative yields in noncondensable gaseous products, while the basic oxides did not have such an effect significantly. Therefore, the role of acidity from metal oxides mainly influences the catalytic cracking of long-chain polymers to small hydrocarbon compounds and gaseous products. The results showed that the blending of AC with spent FCC at a mass ratio of 0.5:0.5 slightly increased the liquid product yields from 82.08 to 82.11 wt % and increased the gas product yields from 10.76 to 14.01 wt %, whereas the solid product yield also significantly decreased from 7.16 to 3.88 wt % by increasing the spent FCC-AC loading from 1 to 5 wt %. This affected the role of both Brønsted and Lewis acid active sites in FCC and facilitated carbon−carbon bond cleavage to small hydrocarbon compounds, while the strong ability of AC to decompose long-chain polymers to aromatic hydrocarbons with hydrogen release.[21−23,27] C−C bond cleavage also occurred on the pore surface structure of AC for the conversion of long-chain
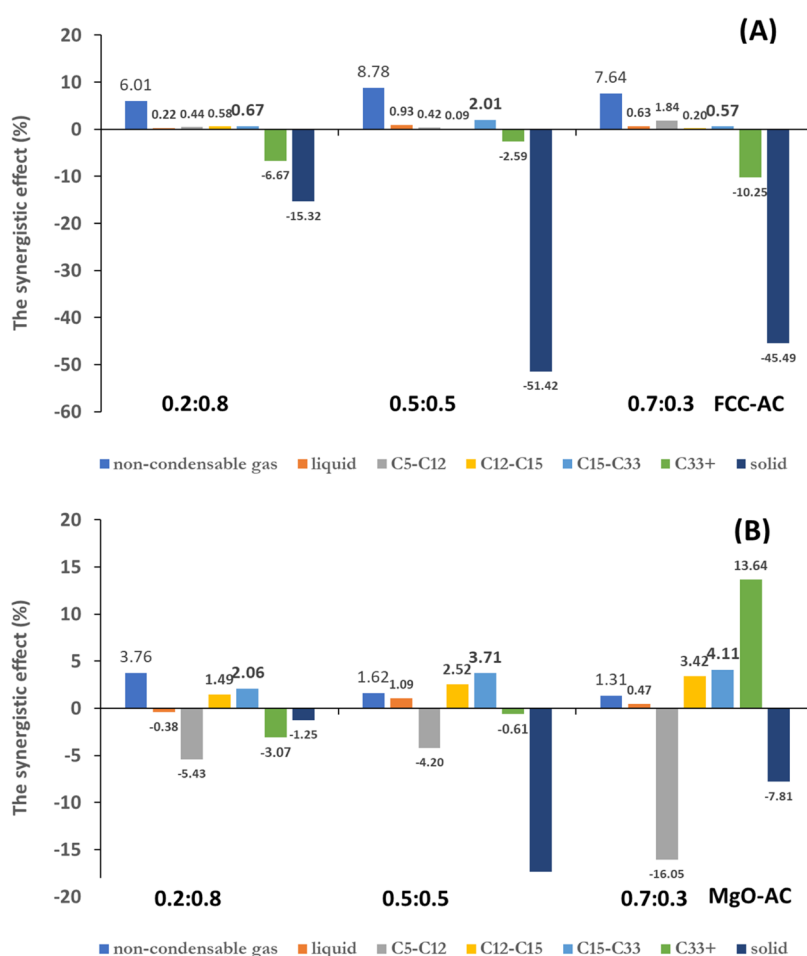
Figure 8. Difference in experimental yield vs theoretical yield by blending activated carbon with spent FCC and MgO: (A) FCC-AC (B) MgO-AC.

hydrocarbons into medium-length compounds, i.e., naphtha-like compounds increased from 28.89 to 29.78 wt % and kerosene-like compounds increased from 13.71 to 13.18 wt %, while the diesel-like fraction did not significantly decrease from 35.66 to 35.56 wt % because the use of spent FCC enhanced C−C bond cleavage and promoted hydrogen transfer to engage the decomposition of long-chain hydrocarbons, followed by a secondary cleavage reaction to form small hydrocarbon compounds in the naphtha-like range.[17,18,22]

Moreover, the blending of AC with MgO at a mass ratio of 0.5:0.5 showed that the liquid product yields that were slightly increased from 82.80 to 82.95 wt %, and the gas product yields increased from 9.94 to 10.83 wt %, whereas the solid product yield moderately decreased from 7.86 to 6.22 wt % when increasing the spent MgO-AC loading from 1 to 5 wt %, which affected the influence of temperature on the promotion of radicals and β-scission of long-chain polymers into small hydrocarbons. The role of MgO, which has a relatively large pore size and conducive ability to the production of medium-length hydrocarbon compounds, including the mesoporous structure and lower specific surface area of MgO, resulted in a mass transfer of pyrolytic volatiles on the MgO surface area and insufficient heat transfer to the cleavage of carbon−carbon bonds, resulting in the formulation of fewer hydrogen and hydrocarbon radicals[20,26,28,30,34] to obtain small hydrocarbon compounds and increase the yield of naphtha-like compounds from 27.29 to 21.60 wt %, and the yield of diesel-like

compounds increased from 36.91 to 41.92 wt %. When the MgO-AC loading was increased from 1 to 5 wt %.

3.4. Synergistic Study of Blended AC Catalysts. To understand the synergistic effect of AC blended with spent FCC and MgO to determine the possible reaction mechanism during catalytic pyrolysis of WPEW, the calculated and experimental product distributions are also listed in Table S10. As seen in Figure 8A, from the difference in the actual and theoretical yields of the product distribution when using the blended AC with spent FCC at various ratios, it is worth noting that the noncondensable gas and diesel-like compounds have a positive synergistic effect. Both the actual and theoretical noncondensable gas yields increased and then decreased with decreasing FCC-AC ratio, indicating that there was a positive effect on noncondensable gas yield with increasing active Brønsted and Lewis acid sites from spent FCC, which promoted an active carbocation and further cleavage reactions into small hydrocarbon compounds and produced a large gas product yield. Moreover, AC has a mesoporous and high surface area; therefore, the small noncondensable gas compounds also reacted with the acid site and rapidly diffused through the mesopores of AC. As seen from the results, the combination of spent FCC-AC presented quite a positive effect on the diesel-like yield, where the blending of AC with FCC can be explained by the high proportion of active acid sites from both acid−acid catalysts enhancing the promotion of C−C bond cleavage to small hydrocarbon compounds. Isomerization, oligomerization, and

Table 3. GC-MS Analyses of Pyrolyzed Oil

peak no.	% area peak					chemical compounds	molecular formula
	FCC	MgO	AC	FCC-AC	MgO-AC		
paraffins	69.921	62.871	68.976	69.776	65.734		
1	1.122	0.049	0.967	1.115	0.096	heptane	C_7H_{16}
2	2.350	1.207	1.436	2.232	0.657	octane	C_8H_{18}
3	2.023	1.163	1.625	2.006	1.087	nonane	C_9H_{20}
4	3.036	2.031	2.399	2.764	1.275	decane	$C_{10}H_{22}$
5	3.245	1.635	2.600	3.135	1.892	undecane	$C_{11}H_{24}$
6	0.115	0.123	0.127	0.115	0.153	5-methyl-undecane	$C_{12}H_{26}$
7	0.000	0.095	0.079	0.038	0.098	3-methyl-undecane	$C_{12}H_{26}$
8	8.178	4.417	4.594	5.918	2.506	dodecane	$C_{12}H_{26}$
9	5.853	2.108	3.233	5.315	2.434	tridecane	$C_{13}H_{28}$
10	0.161	0.178	0.225	0.115	0.181	2,4-dimethyldodecane	$C_{14}H_{30}$
11	0.000	0.040	0.098	0.149	0.079	2,3-dimethyldodecane	$C_{14}H_{30}$
12	0.094	0.462	0.176	0.063	0.327	7-methyl-heptadecane	$C_{18}H_{38}$
13	6.521	5.985	7.089	7.118	5.555	tetradecane	$C_{14}H_{30}$
14	0.131	0.123	0.101	0.000	0.132	4-methy-tetradecane	$C_{15}H_{32}$
15	0.000	0.078	0.096	0.094	0.109	3-methyl-tetradecane	$C_{15}H_{32}$
16	4.763	2.198	3.715	4.635	3.887	hexadecane	$C_{16}H_{34}$
17	0.000	0.000	0.116	0.089	0.093	2,6,10,14-tetramethyl-hexadecane	$C_{20}H_{42}$
18	0.319	0.312	0.159	0.174	0.256	5-methyl-tetradecane	$C_{15}H_{32}$
19	2.885	2.172	0.100	2.128	1.874	hexadecane	$C_{16}H_{34}$
20	0.552	0.125	0.163	0.039	0.182	3-methyl-pentadecane	$C_{16}H_{34}$
21	5.139	3.485	7.586	4.073	7.024	heptadecane	$C_{17}H_{36}$
22	0.203	0.036	0.076	0.115	0.076	5-methyl-tetradecane	$C_{15}H_{32}$
23	0.098	0.144	0.135	0.046	0.168	2-methy-hexadecane	$C_{17}H_{36}$
24	2.425	2.839	3.622	3.340	4.076	heptadecane	$C_{17}H_{36}$
25	1.533	0.173	0.166	0.994	0.204	pentadecane	$C_{21}H_{44}$
26	0.115	0.095	0.119	0.069	0.135	2-methyl-heptadecane	$C_{18}H_{38}$
27	0.000	0.238	0.132	0.117	0.204	3-methyl-heptadecane	$C_{18}H_{38}$
28	3.778	6.147	6.682	6.920	6.483	heptadecane	$C_{17}H_{36}$
29	2.542	3.104	3.080	4.116	4.334	eicosane	$C_{20}H_{42}$
30	0.093	0.091	0.134	0.095	0.145	2,4-dimethyl-eicosane	$C_{22}H_{46}$
31	0.111	0.145	0.124	0.110	0.159	9-octyl-heptadecane	$C_{25}H_{52}$
32	4.156	5.646	5.469	2.982	4.715	eicosane	$C_{20}H_{42}$
33	0.569	0.663	0.086	0.084	0.342	2-methylhexacosane	$C_{27}H_{56}$
34	2.057	2.592	2.294	2.115	2.092	heneicosane	$C_{21}H_{44}$
35	0.117	0.189	0.103	0.225	0.160	5-methyl-heneicosane	$C_{22}H_{46}$
36	2.673	3.939	3.836	2.120	3.941	heneicosane	$C_{21}H_{44}$
37	2.324	3.773	1.403	3.029	2.679	tetracosane	$C_{24}H_{50}$
38	0.000	1.226	2.225	0.000	2.291	tetracosane	$C_{24}H_{50}$
39	0.117	0.669	0.638	0.452	0.752	docosane	$C_{22}H_{46}$
40	0.000	0.887	1.172	1.054	1.306	hexatriacontane	$C_{36}H_{74}$
41	0.523	2.032	0.275	0.478	1.057	hexatriacontane	$C_{36}H_{74}$
42	0.000	0.257	0.521	0.000	0.517	hexatriacontane	$C_{36}H_{74}$
olefin	27.961	29.888	26.863	24.054	27.049		
43	2.117	1.882	0.780	2.099	0.086	1-heptene	C_7H_{14}
44	3.224	1.022	1.235	2.181	1.901	1-octene	C_8H_{16}
45	1.187	2.098	1.618	1.228	1.688	1-nonene	C_9H_{18}
46	1.935	2.730	2.167	1.228	1.315	1-decene	$C_{10}H_{20}$
47	0.000	1.117	0.120	0.123	0.049	trans-3-decene	$C_{10}H_{20}$
48	2.398	1.253	2.499	2.210	2.461	1-undecene	$C_{11}H_{22}$
49	0.000	0.238	0.152	0.139	0.648	(E)-2-undecene	$C_{11}H_{22}$
50	0.000	0.036	0.073	0.089	0.088	(E)-3-dodecene	$C_{12}H_{24}$
51	2.331	3.221	2.806	1.282	2.721	1-dodecene	$C_{12}H_{24}$
52	0.000	0.120	0.178	0.154	0.134	(Z)-2-dodecene	$C_{12}H_{24}$
53	0.000	0.038	0.099	0.126	0.080	(E)-3-tetradecene	$C_{14}H_{28}$
54	2.132	1.759	2.730	1.865	2.268	1-tridecene	$C_{13}H_{26}$
55	0.152	1.239	0.181	0.123	1.061	1-tridecene	$C_{13}H_{26}$
56	0.097	0.095	0.138	0.125	0.078	(Z)-3-hexadecene	$C_{16}H_{32}$
57	3.258	2.630	2.740	1.393	2.827	1-tetradecene	$C_{14}H_{28}$

Table 3. continued

peak no.	% area peak					chemical compounds	molecular formula
	FCC	MgO	AC	FCC-AC	MgO-AC		
58	0.000	0.128	0.216	0.156	0.218	1-tetradecene	$C_{14}H_{28}$
59	0.077	0.841	0.168	0.118	0.903	(Z)-3-hexadecene	$C_{16}H_{32}$
60	2.345	1.389	2.241	2.374	1.265	1-pentadecene	$C_{15}H_{30}$
61	0.012	0.673	0.311	0.128	0.082	1-pentadecene	$C_{15}H_{30}$
62	3.113	0.122	0.156	2.221	0.197	1-pentadecene	$C_{15}H_{30}$
63	1.434	1.239	1.704	1.456	1.437	1-heptadecene	$C_{17}H_{34}$
64	0.000	1.226	1.263	0.000	1.919	1-heptadecene	$C_{17}H_{34}$
65	0.132	0.126	0.232	0.254	0.562	3-heptadecene	$C_{17}H_{34}$
66	0.097	0.749	0.122	0.000	0.084	(Z)-3-heptadecene	$C_{17}H_{34}$
67	1.013	0.674	0.848	1.098	0.951	1-nonadecene	$C_{19}H_{38}$
68	0.098	0.112	0.127	0.173	0.134	1-nonadecene	$C_{19}H_{38}$
69	0.452	0.632	0.605	0.485	0.357	1-nonadecene	$C_{19}H_{38}$
70	0.119	0.130	0.149	0.191	0.124	1-nonadecene	$C_{19}H_{38}$
71	0.037	0.399	0.074	0.119	0.075	1-nonadecene	$C_{19}H_{38}$
72	0.039	0.058	0.090	0.121	0.079	1-tetracosene	$C_{24}H_{48}$
73	0.014	0.584	0.447	0.399	0.434	1-nonadecene	$C_{19}H_{38}$
74	0.000	0.221	0.277	0.086	0.168	1-nonadecene	$C_{19}H_{38}$
75	0.000	0.175	0.197	0.094	0.196	1-nonadecene	$C_{19}H_{38}$
76	0.148	0.932	0.120	0.217	0.459	1-hexacosene	$C_{26}H_{52}$
cyclic paraffins	2.005	7.212	4.068	6.157	7.184		
77	1.013	1.038	1.903	1.370	1.101	methyl-cyclopentane	C_6H_{12}
78	0.252	1.198	0.127	0.139	1.062	cyclohexane	C_6H_{12}
79	0.041	0.687	0.090	0.091	0.088	methyl-cyclohexane	C_7H_{14}
80	0.000	0.135	0.093	0.880	0.128	3-hexyl-1,1-dimethyl-cyclopentane	$C_{13}H_{26}$
81	0.215	0.471	0.149	1.031	0.325	hexyl-cyclopentane	$C_{11}H_{22}$
82	0.117	0.906	0.165	0.985	0.371	1,2-dibutyl-cyclopentane	$C_{13}H_{26}$
83	0.043	0.073	0.068	0.109	0.127	n-nonylcyclohexane	$C_{15}H_{30}$
84	0.032	0.349	0.507	0.128	0.537	cyclohexadecane	$C_{16}H_{32}$
85	0.185	0.227	0.196	1.040	0.122	cyclohexadecane	$C_{16}H_{32}$
86	0.000	0.239	0.203	0.141	0.069	4-cyclohexyl-tridecane	$C_{19}H_{38}$
87	0.107	0.209	0.253	0.029	1.926	4-cyclohexyl-tridecane	$C_{19}H_{38}$
88	0.000	1.680	0.128	0.090	1.292	4-cyclohexyl-undecane	$C_{17}H_{34}$
cyclic olefins	0.113	0.000	0.093	0.012	0.018		
89	0.113	0.000	0.093	0.112	0.018	1-methyl-cyclopentene	C_6H_{10}
90	0.000	0.029	0.000	0.000	0.015	3-methyl-cyclopentene	C_6H_{10}

further secondary cracking reactions of small hydrocarbons may occur at the active site of the catalyst surface and form hydrocarbon compounds in the C_5-C_{32} range. The results associated with a radical and a carbocation enhanced successive catalytic cleavage to obtain small hydrocarbons and medium-length hydrocarbons that were promoted during the thermal reaction, catalytic reaction, and secondary cracking reaction when using both via the active acid–acid catalyst.

Figure 8B shows that the synergistic effect on diesel-like yield may be affected by the MgO catalyst, which had both a Lewis basic structure and a mesoporous surface structure enhancing the contribution of C–C bond cleavage into a medium-length hydrocarbon chain, which indicated that the use of MgO promoted the generation of a noncondensable gas and liquid product in the $C_{18}-C_{32}$ range. Then, medium-length hydrocarbon compounds were observed during the use of only MgO in catalysis pyrolysis and further reacted with the active Brønsted and Lewis acid sites through the mesoporous position of AC, which had a large surface area. Therefore, the possible chemical mechanism is also associated with radicals and porosity with a large surface area of activated carbon promoting the synergistic effect of these characteristics on the liquid yield of diesel-like compounds.

3.5. Characterization of Chemical Compounds and Physicochemical Properties. Table 3 represents the approximate percentage of the relative peak area from GC-MS analyses that matched the NIST chemical library, which was divided into four groups (paraffins, olefins, cyclic paraffins, and cyclic olefins). The GC-MS analyses of catalytic pyrolysis oil using a spent FCC mainly consisted of paraffins (69.921%) and olefins (27.961%), which contained carbon atom distributions ranging from 6 to 36 atoms. When dividing the carbon atoms from GC-MS analyses into naphtha-like (C_5-C_{12}), kerosene-like and diesel-like ranges, it was found that the main compounds were decane ($C_{10}H_{22}$, 3.036%), dodecane ($C_{12}H_{26}$, 8.178%), and heptadecane ($C_{17}H_{36}$, 5.139%). This was caused by the Brønsted and Lewis acid sites of spent FCC promoting the further catalytic cleavage of long-chain radicals from thermal cleavage into small hydrocarbon chains, and then oligomerization and isomerization reactions of medium-length hydrocarbons occurred on the pore surface structure to produce a linear unsaturated hydrocarbon in the range of C_5-C_{18}. The blending of AC, which has a weak acid active site with a mesoporous structure and large surface area, enhanced the decomposition of medium-length hydrocarbons to both linear saturated and unsaturated hydrocarbons.[22,32−35]

Table 4. Physicochemical Analyses of Pyrolysis Oil

typical analysis	FCC	MgO	AC	FCC-AC	MgO-AC	diesel[1,37,38]	method of analysis
higher heating value (MJ kg^{-1})	45.1	42.8	44.2	44.7	44.1	42.8−45.8	ASTM-D240
kinematic viscosity at 40 °C (mm^2 s^{-1})	1.9	1.5	1.7	1.7	1.7	1.4−1.9	ASTM-D445-19
acidity (mg$_{KOH}$ g^{-1})	0	0	0	0	0	0	ASTM-D664-07

The catalytic pyrolysis of WPEW using MgO-AC at a temperature of 420 °C, a flow rate of inert N$_2$ at 50 mL min^{-1}, and a catalyst loading at 5 wt % obtained a product distribution mainly in the diesel-like fraction. GC-MS analyses showed the presence of typical hydrocarbon compounds, mainly paraffins (65.734%) and olefins (27.049%), which contain carbon atom distributions ranging from 6 to 36 atoms. When dividing the carbon atoms from GC-MS analyses into the naphtha-like range (C$_5$−C$_{12}$), kerosene-like range (C$_{12}$−C$_{15}$), and diesel-like range (C$_{15}$−C$_{33}$), it was found that the main compositions were undecane (C$_{11}$H$_{24}$, 1.892%), tetradecane (C$_{14}$H$_{30}$, 5.555%), and heptadecane (C$_{17}$H$_{36}$, 7.024%). Furthermore, GC-MS analyses of catalytic pyrolysis of WPEW using MgO-AC catalysts exhibited mainly chemical compounds in the desirable diesel-like range, causing the thermal degradation to produce a volatile vapor, resulting in the cleavage of carbon−carbon bonds on the main chain, and branched chains obtained hydrogen radicals and short hydrocarbon radicals, after which a volatile vapor diffused through the MgO catalyst and initiated catalytic cleavage on the pore surface structure. Afterward, linear paraffins/olefins were produced from the hydrogen transfer and breakage of radical reactions to obtain a long residue range (C$_{33}^+$). Then, AC converted long-chain hydrocarbons to linear paraffins with hydrogen released during the reaction process.[22,33−35] The cleavage of carbon−carbon bonds occurring on the surface of AC enhances the conversion of long-chain hydrocarbons into diesel-like hydrocarbons (C$_{17}$−C$_{32}$) and dehydrogenation into gas product yield with the terminating step of hydrogen radicals.[22,26,27] Furthermore, it was also found that no aromatic hydrocarbon compounds were present due to the weakly acidic sites of AC that could not facilitate the aromatization reaction to produce aromatic compounds, but the AC catalyst enhanced the successive cyclization reaction of linear alkanes, resulting in the production of cyclic paraffins and cyclic olefins.

Physicochemical analyses of pyrolysis oil in terms of heating value, kinematic viscosity, acidity, and methods of analysis are listed in Table 4. The catalytic pyrolysis of WPEW using MgO-AC produced the highest yield in the diesel-like fraction, with a calorific value, kinematic viscosity at 40 °C, and modification acid number of 44.20 MJ kg^{-1}, 1.7 mm^2 s^{-1}, and no acid value, respectively. When comparing spent FCC and MgO, the blending of AC into spent FCC and MgO catalysts beneficially produced a desired product in the diesel-like range because the large surface area promoted the catalytic reaction at the pore surface structure to accelerate the decomposition of the polymer, including the effect of mesoporous enhanced isomerization and oligomerization of medium-length hydrocarbon compounds, which can be adjusted according to various desired products that can be utilized as alternative energy sources; thus, this technique is a practical route to be studied further to meet the Bio-Circular-Green Economy model toward sustainability.

4. CONCLUSIONS

WPEW was converted into diesel-like oil through thermal decomposition in the process temperature range of 400−470 °C. The use of individual catalysts, such as spent FCC, MgO, and AC and blended catalysts, also increased both the liquid yield and diesel-like oil yield. The highest liquid and diesel-like fraction yields of 82.95 and 41.92 wt %, respectively, were obtained at the process temperature of 420 °C using the combination of AC and MgO at a ratio of 0.5:0.5, while the use of both spent FCC-AC and MgO-AC exhibited positive synergy due to strong Lewis acids and strong Lewis base catalysts enhancing the decomposition of long-chain hydrocarbon compounds to smaller hydrocarbons via catalytic activity to achieve aliphatic paraffins, olefins, and aromatic compounds through isomerization, oligomerization, cyclization, and aromatization reactions. Pyrolysis yielded oil in the boiling range of diesel-like compounds (C$_5$−C$_{18}$). The results of the characterization showed that the oil obtained under optimum conditions had a calorific value, kinematic viscosity at 40 °C, and modification acid number of 44.20 MJ kg^{-1}, 1.7 mm^2 s^{-1}, and no acid value, respectively. The catalytic pyrolysis from WPEW makes it a viable alternative fuel source and may be applied to completely convert waste into sustainable, high-value chemicals, including decomposing the waste prior to end product extraction.

■ ASSOCIATED CONTENT

Ⓢ Supporting Information

The Supporting Information is available free of charge at https://pubs.acs.org/doi/10.1021/acsomega.2c02301.

Effect of operating pyrolysis conditions on product distribution and the synergistic effect of the catalyst blended (PDF)

■ AUTHOR INFORMATION

Corresponding Author

Witchakorn Charusiri − Faculty of Environmental Culture and Ecotourism, Srinakharinwirot University, Bangkok 10110, Thailand; ⓞ orcid.org/0000-0002-4058-0367; Email: witchakorn@swu.ac.th

Authors

Piyaporn Kasetsupsin − Department of Chemical Technology, Faculty of Science, Chulalongkorn University, Bangkok 10330, Thailand

Tharapong Vitidsant − Department of Chemical Technology, Faculty of Science, Chulalongkorn University, Bangkok 10330, Thailand; Center of Excellence on Petrochemical and Materials Technology, Chulalongkorn University, Bangkok 10330, Thailand

Aminta Permpoonwiwat − Patumwan Demonstration School, Srinakharinwirot University, Bangkok 10330, Thailand

Naphat Phowan − Faculty of Environmental Culture and Ecotourism, Srinakharinwirot University, Bangkok 10110, Thailand

Complete contact information is available at:
https://pubs.acs.org/10.1021/acsomega.2c02301

Author Contributions

P.K. contributed to conceptualization, experiment, formal analysis, investigation, visualization, and writing—original draft. T.V. contributed to conceptualization, supervision, and validation. A.P. performed visualization and writing—original draft. N.P. carried out formal analysis and visualization. W.C. contributed to conceptualization, supervision, methodology, formal analysis, validation, visualization, writing—review & editing, and funding acquisition.

■ REFERENCES

(1) Anuar Sharuddin, S. D.; Abnisa, F.; Wan Daud, W. M. A.; et al. A review on pyrolysis of plastic wastes. *Energy Convers. Manage.* 2016, *115*, 308−326.

(2) Liu, Y.; Fu, W.; Liu, T.; et al. Microwave pyrolysis of polyethylene terephthalate (PET) plastic bottle sheets for energy recovery. *J. Anal. Appl. Pyrolysis* 2022, *161*, No. 105414.

(3) Arabiourrutia, M.; Elordi, G.; Lopez, G.; et al. Characterization of the waxes obtained by the pyrolysis of polyolefin plastics in a conical spouted bed reactor. *J. Anal. Appl. Pyrolysis* 2012, *94*, 230−237.

(4) Dai, L.; Zhou, N.; Li, H.; et al. Catalytic fast pyrolysis of low density polyethylene into naphtha with high selectivity by dual-catalyst tandem catalysis. *Sci. Total Environ.* 2021, *771*, No. 144995.

(5) Jha, K. K.; Kannan, T.T.M.; Senthilvelan, N. Optimization of catalytic pyrolysis process for change of plastic waste into fuel. *Mater. Today: Proc.* 2021, *39*, 708−711.

(6) Rodríguez-Luna, L.; Bustos-Martínez, D.; Valenzuela, E. Two-step pyrolysis for waste HDPE valorization. *Process Saf. Environ. Prot.* 2021, *149*, 526−536.

(7) Chaiya, C.; Pankumpet, N.; Buapibal, B.; et al. Alternative liquid fuel from pyrolysis of polyethylene wax. *Energy Rep.* 2020, *6*, 1262−1267.

(8) Parku, G. K.; Collard, F.; F Görgens, J. Pyrolysis of waste polypropylene plastics for energy recovery: Influence of heating rate and vacuum conditions on composition of fuel product. *Fuel Process. Technol.* 2020, *209*, No. 106522.

(9) Saeaung, K.; Phusunti, N.; Phetwarotai, W.; et al. Catalytic pyrolysis of petroleum-based and biodegradable plastic waste to obtain high-value chemicals. *Waste Manage.* 2021, *127*, 101−111.

(10) Santos, E.; Rijo, B.; Lemos, F.; et al. A catalytic reactive distillation approach to high density polyethylene pyrolysis − Part 2 − Middle olefin production. *Catal. Today* 2021, *379*, 212−221.

(11) Lee, K.-H. Effects of the types of zeolites on catalytic upgrading of pyrolysis wax oil. *J. Anal. Appl. Pyrolysis* 2012, *94*, 209−214.

(12) Aboul-Enein, A. A.; Soliman, F. S.; Betiha, M. A. Co-production of hydrogen and carbon nanomaterials using NiCu/SBA15 catalysts by pyrolysis of a wax by-product: Effect of Ni−Cu loading on the catalytic activity. *Int. J. Hydrogen Energy* 2019, *44*, 31104−31120.

(13) Arandes, J. M.; Azkoiti, M. J.; Torre, I.; et al. Effect of HZSM-5 catalyst addition on the cracking of polyolefin pyrolysis waxes under FCC conditions. *Chem. Eng. J.* 2007, *132*, 17−26.

(14) Arandes, J. M.; Torre, I.; Azkoiti, M. J.; et al. Effect of catalyst properties on the cracking of polypropylene pyrolysis waxes under FCC conditions. *Catal. Today* 2008, *133−135*, 413−419.

(15) Hwang, K.-R.; et al. Catalytic cracking of chlorinated heavy wax from pyrolysis of plastic wastes to low carbon-range fuels: Catalyst effect on properties of liquid products and dichlorination. *J. Anal. Appl. Pyrolysis* 2021, *115*, No. 105090.

(16) Yu, J.; Liu, S.; Cardoso, A.; et al. Catalytic pyrolysis of rubbers and vulcanized rubbers using modified zeolites and mesoporous catalysts with Zn and Cu. *Energy* 2019, *188*, No. 116117.

(17) Chen, X.; Ren, L.; Yaseen, M.; et al. Synthesis, characterization and activity performance of nickel-loaded spent FCC catalyst for pine gum hydrogenation. *RSC Adv.* 2019, *9*, 6515−6525.

(18) Rodríguez, E.; Gutiérrez, A.; Palos, R.; et al. Fuel production by cracking of polyolefins pyrolysis waxes under fluid catalytic cracking (FCC) operating conditions. *Waste Manage.* 2019, *93*, 162−172.

(19) Charusiri, W.; Vitidsant, T. Upgrading bio-oil produced from the catalytic pyrolysis of sugarcane (*Saccharum officinarum* L) straw using calcined dolomite. *Sustainable Chem. Pharm.* 2017, *6*, 114−123.

(20) Dai, L.; Zhou, N.; Lv, Y.; et al. Pyrolysis-catalysis for waste polyolefin conversion into low aromatic naphtha. *Energy Convers. Manage.* 2021, *245*, No. 114578.

(21) Huo, E.; Lei, H.; Liu, C.; et al. Jet fuel and hydrogen produced from waste plastics catalytic pyrolysis with activated carbon and MgO. *Sci. Total Environ.* 2020, *727*, No. 138411.

(22) Zhang, Y.; Duan, D.; Lei, H.; et al. Jet fuel production from waste plastics via catalytic pyrolysis with activated carbons. *Appl. Energy* 2019, *251*, No. 113337.

(23) Alonso-Fariñas, B.; Rodríguez-Galán, M.; Arenas, C.; et al. Sustainable management of spent fluid catalytic cracking catalyst from a circular economy approach. *Waste Manage.* 2020, *110*, 10−19.

(24) Suprianto, T.; Wijayanti, W.; Wardana, I.; et al. Synergistic effect of curcumin and activated carbon catalyst enhancing hydrogen production from biomass pyrolysis. *Int. J. Hydrogen Energy* 2021, *46*, 7147−7164.

(25) Jiang, L.; et al. Characteristics and synergistic effects of co-pyrolysis of microalgae with polypropylene. *Fuel* 2021, *314*, No. 122765.

(26) Hong, D.; Gao, P.; Wang, C. A comprehensive understanding of the synergistic effect during co-pyrolysis of polyvinyl chloride (PVC) and coal. *Energy* 2022, *239*, No. 122258.

(27) Osman, A. I.; Blewitt, J.; Abu-Dahrieh, J. K.; et al. Production and characterisation of activated carbon and carbon nanotubes from potato peel waste and their application in heavy metal removal. *Environ. Sci. Pollut. Res.* 2019, *26*, 37228−37241.

(28) Zhu, Z.; Liu, Y.; Cong, W.; et al. Soybean biodiesel production using synergistic CaO/Ag nano catalyst: Process optimization, kinetic study, and economic evaluation. *Ind. Crops Prod.* 2021, *166*, No. 113479.

(29) Lovás, P.; Hudec, P.; Jambor, B.; et al. Catalytic cracking of heavy fractions from the pyrolysis of waste HDPE and PP. *Fuel* 2017, *203*, 244−252.

(30) Ahmad, I.; Khan, M. I.; Khan, H.; et al. Pyrolysis study of polypropylene and polyethylene into premium oil products. *Int. J. Green Energy* 2015, *12*, 663−671.

(31) Pihl, O.; Khaskhachikh, V.; Kravetskaja, J.; et al. Co-pyrolysis of estonian oil shale with polymer wastes. *ACS Omega* 2021, *6*, 31658−31666.

(32) Jin, X.; Lee, J. H.; Choi, J. W. Catalytic co-pyrolysis of woody biomass with waste plastics: Effects of HZSM-5 and pyrolysis temperature on producing high-value pyrolytic products and reducing wax formation. *Energy* 2022, *239*, No. 121739.

(33) Nakaji, Y.; Tamura, M.; Miyaoka, S.; et al. Low-temperature catalytic upgrading of waste polyolefinic plastics into liquid fuels and waxes. *Appl. Catal., B* 2021, *285*, No. 119805.

(34) Xue, Q.; Li, Z.; Jiang, Z.; et al. Diesel reforming to hydrogen over the mesoporous Ni−MgO catalyst synthesized in microfluidic platform. *Int. J. Hydrogen Energy* 2021, *46*, 36709−36720.

(35) Bozkurt, P. A.; Tosun, O.; Canel, M. The synergistic effect of co-pyrolysis of oil shale and low density polyethylene mixtures and characterization of pyrolysis liquid. *J. Energy Inst.* **2017**, *90*, 355−362.

(36) Charusiri, W.; Vitidsant, T. Response surface methodology optimization of biofuels produced by catalytic pyrolysis of residual palm oil from empty fruit bunch over magnesium oxide. *J. Chem. Eng. Jpn.* **2017**, *50*, 727−736.

(37) Hu, Z.; Ma, X.; Li, L. The synergistic effect of co-pyrolysis of oil shale and microalgae to produce syngas. *J. Energy Inst.* **2016**, *89*, 447−455.

(38) Chang, J.-S.; Cheng, J. C.; Ling, T. R.; et al. Low acid value bio-gasoline and bio-diesel made from waste cooking oils using a fast pyrolysis process. *J. Taiwan Inst. Chem. Eng.* **2017**, *73*, 1−11.